JMEPEG (2023) 32:5620–5626
https://doi.org/10.1007/s11665-022-07506-9

©ASM International
1059-9495/$19.00

TECHNICAL ARTICLE

Effect of Mg Content on the Microstructure and Comprehensive Properties of Al-5Si-5.3Cu-0.3Sr-0.2Zr-0.2Y-0.06Ti-*x*Mg Alloy

Zhiheng Hong, Hao Wang, Xiaojing Xu, and Lele Liu

Submitted: 5 July 2022 / Revised: 18 September 2022 / Accepted: 25 September 2022 / Published online: 10 October 2022

In this study, the effects of magnesium addition on the microstructure and comprehensive properties of Al-5Si-5.3Cu-0.3Sr-0.2Zr-0.2Y-0.06Ti alloys were investigated by optical microscope, scanning electron microscope, transmission electron microscope, hardness tester, and tensile testing machine. It is found that the addition of magnesium increases the number of undissolved particles in the alloy. However, on the one hand, magnesium addition refines the θ' phase and increases its number density in the alloy. On the other hand, it generates a smaller Q′ phase. Both phases can enhance the precipitation strengthening and dislocation strengthening of the alloy. In addition, adding magnesium reduces the width of the precipitation-free zone (PFZ) and changes the distribution of grain boundary precipitates (GBPs). At 1% magnesium addition, the dislocation strengthening and precipitation strengthening effects of the θ' and Q′ phases were the best, the width of PFZ was the smallest, and the GBPs were discontinuously arranged along the PFZ. Therefore, a high-strength, high-hardness, and intergranular corrosion-resistant cast aluminum alloy with dense structure, a tensile strength of 364.4 MPa, elongation of 4.87%, hardness of 145.4 HV, and intergranular corrosion grade of 3 was obtained.

Keywords Al-Si-Cu alloy, comprehensive properties, microstructure, microalloying

1. Introduction

Al-Si-Cu alloy is a commonly used die-casting Al-Si alloy, which can be strengthened by heat treatment to improve mechanical properties and is usually used in automobile cylinder blocks and cylinder heads (Ref 1-5). Microalloying is usually used to improve the microstructure and comprehensive properties of Al-Si-Cu alloys to obtain Al-Si-Cu alloys′ better properties (Ref 1, 4). Magnesium (Mg) is a microalloying element commonly used in aluminum alloys (Ref 6, 7). Magnesium addition can slightly refine the sizes of α-Al and eutectic Si (Ref 8). When magnesium is added to Al-Si-Cu alloy, the main strengthening precipitations in the alloy become the Q/Q′ and θ'/θ-Al_2Cu phases (Ref 6, 9-11). The aging precipitation sequence of Al-Si-Cu-Mg alloy is as follows: (Ref 12)

$$\text{ass} \rightarrow \text{GPZ} \rightarrow \theta'' \rightarrow \theta' \rightarrow \theta\text{ass} \rightarrow \text{Q}'' \rightarrow \text{Q}' \rightarrow \text{Q}$$

Existing research has shown that the precipitation of a high-density fine Q′ phase occurs before the θ' phase, thereby becoming an obstacle to the movement of dislocations, which is conducive to improving the strength of the alloy and profoundly impacts its hardness. The hardness is enhanced due to the coexistence of dominant Q′ and θ' phases in the peak-aged state when the high-density fine Q′ phase precipitates before the θ' phase (Ref 7). Hao et al. Ref 12 found that the precipitated Q′ phase is partially coherent with the Al matrix, resulting in lattice distortion, which enhances the strength of the alloy. In addition to enhancing the hardness and strength of the alloy, the Q′ phase also improves the corrosion resistance of Al-Si-Cu-Mg alloy with high copper (Cu) content. In Al-Si-Cu-Mg alloys with high Cu content, the corrosion resistance of the alloy can be improved by forming discontinuous Q′ precipitates at grain boundaries (Ref 13). In general, the structure of Q′ in Al-Si-Cu-Mg alloy is generally smaller because Cu atoms are gradually segregated to the Q′/α-Al interface during aging, which inhibits the coarsening of the Q′ precipitation (Ref 14). Q is an equilibrium phase that precipitates after Q′ (Ref 12). There are strong mixed covalent-ionic TM-Si bonds in the Q phase, which is beneficial to increase the hardness of the alloy (Ref 15). Farkoosh et al. Ref 6 found that higher amounts of Q precipitation produced Orowan strengthening to increase strength.

The introduced Q phase or Q′ phase and the transformation of other phases by adding magnesium into the Al-Si-Cu alloy have a beneficial effect on alloy properties, which indicates the significance of magnesium addition on Al-Si-Cu alloys. Accordingly, the effects of various Mg contents on Al-Si-Cu alloys were investigated in the present study.

Zhiheng Hong, Hao Wang, Xiaojing Xu, and **Lele Liu**, Institute of Advanced Manufacturing and Modern Equipment Technology, Jiangsu University, Zhenjiang 212013 Jiangsu, China. Contact e-mail: yjs_xx@126.com.

2. Experimental

2.1 Alloy Preparation

Table 1 shows the specific composition of the alloy. The melting and heat-treatment process of Al-5Si-5.3Cu-0.3Sr-0.2Zr-0.2Y-0.06Ti-xMg alloy was as follows. First, pure Al (99.79%Al) and Al-Cu (50.12%Cu), Al-Si (20%Si), and Al-Ti-B (5.11%Ti) master alloys were placed in a graphite crucible in a furnace, whose rated temperature was set to 850 °C and was kept for 2 h. The casting mold was heated. C_2Cl_6 wrapped in tin foil was added for degassing after the above-mentioned raw materials melting. The master alloys of Al-Zr (4.11% Zr), Al-Sr (9.89% Sr), and Al-Y (10% Y) were added, and the temperature was maintained for 3 h. Pure magnesium (99.9%Mg) was added when the temperature dropped to 710 ± 10 °C. Degassing was performed three times at a degassing interval of 10 min, after which it was allowed to stay for 15 min. The slag was then removed, and the melting liquid was cast into an ingot mold. The ingot heat-treatment process was as follows: 470 °C × 2 h + 480 °C × 2 h + 490 °C× 2 h + 500 °C × 2 h + 510 °C × 16 h (Room-Temperature water quench) solid solution + 191 °C × 18 h (air cooling) aging.

2.2 Performance Characterization

The microstructure and properties of Al-5Si-5.3Cu-0.3Sr-0.2Zr-0.2Y-0.06Ti-xMg alloy were analyzed as follows. The material was removed from the mold and cut into samples with a dimension of 10 mm × 10 mm × 5 mm. The samples used for SEM observation, hardness test, and intergranular corrosion test were prepared as above. The samples used for SEM observation and analysis were cleaned with alcohol and then corroded with a corrosion solution of 0.5% HF. FEL Quanta100F scanning electron microscope equipped with energy-dispersive spectrometry (EDS) was used to observe the metallographic structure, precipitation distribution of the aluminum alloy. FEI TECNAI G2 F20 200 kV field emission transmission electron microscope was used to observe intragranular precipitates and grain boundaries. Before the test, the sample to be observed was pre-ground to 0.1 mm, and then, the sample was punched by an electrolytic double spray instrument. Finally, ion thinning was performed. The thinned samples were observed under a TEM, and their microstructure and precipitation-diffraction patterns were analyzed. The results of TEM observation were measured by ImageJ. The hardness test was performed with a HV-1000 digital microhardness tester, and the pressure load was set as 500 gf. Five measurements were taken on different parts of the sample. After obtaining the hardness value, results with more significant errors were removed, and the average value of the remaining data was recorded as the final hardness value of the sample. The room-temperature tensile properties were tested using a WDW-200G tensile testing machine. Tensile specimens were processed as shown in Fig. 1. During the measurement, the maximum tensile-force parameter of the tensile machine was set as 20 kN, and the tensile speed was set as 0.5 mm/min. After stretching, the tensile strength and elongation were calculated. The experimental process of the intergranular corrosion (IGC) test was as follows. The surface of the samples was cleaned with 10% NaOH solution for about 10 min and then placed in 30% HNO_3 solution until the surface was smooth and regained its metallic luster. The samples were ultrasonically cleaned with anhydrous ethanol. The samples were suspended in a beaker containing a corrosive solution (NaCl 57 g/L + H_2O_2 10 mL/L), and then, the beaker was placed in a DHG-9030 blast drying oven at a constant temperature of 35 °C for 6 h. Finally, the XQ-1 metallographic mounting machine was used to metallographically mount the samples. The maximum corrosion depth of the samples after IGC was observed using a 4XC-MS optical microscope.

Table 1 Al-5Si-5.3Cu-0.3Sr-0.2Zr-0.2Y-0.06Ti-xMg alloy composition table

Sample	Si	Cu	Sr	Zr	Ti	Y	Mg	Al
#1	5	5.3	0.3	0.2	0.06	0.2	0	Bal
#2	5	5.3	0.3	0.2	0.06	0.2	0.5	Bal
#3	5	5.3	0.3	0.2	0.06	0.2	1	Bal

3. Results and Discussion

3.1 SEM Analysis

Figure 2 shows the SEM image of Al-5Si-5.3Cu-0.3Sr-0.2Zr-0.2Y-0.06Ti-xMg alloy. Figure 3 shows the surface scans of Al, Si, Cu, and Mg elements of Al-5Si-5.3Cu-0.3Sr-0.2Zr-0.2Y-0.06Ti-1 Mg alloy. It can be observed from Fig. 2 that the alloys exhibit dense structures. Moreover, the size of the eutectic silicon is mostly less than 10 μm, and the distribution is uniform. The morphology of eutectic silicon is primarily worm-like or spherical, with rounded edges and no agglomeration (Ref 4, 16, 17). This shows that the addition of magnesium does not adversely affect the modification effect of Si (Ref 16, 17). Furthermore, it can be seen from Fig. 2 that the main intermetallic compound is θ-Al_2Cu (Ref 17-19). The addition of magnesium increases the amount of undissolved intermetallic compounds in the alloy. Fig. 3 shows that the Cu and Mg elements distribution in the #3 alloy is very uniform and they are distributed mostly in α(Al) phase.

The increase in undissolved intermetallic compounds in the alloy after adding magnesium may be attributed to the following reasons. On the one hand, this may be due to the reaction of Mg with Al, Si, Cu, Y, Fe, and other elements in the alloy to generate some intermetallic compounds (Ref 6, 20). Some intermetallic compounds may be difficult to dissolve in a solid solution, so the number of undissolved particles increases. On the other hand, the addition of magnesium will cause the segregation of the Cu phase in the alloy (Ref 21). It is easy to

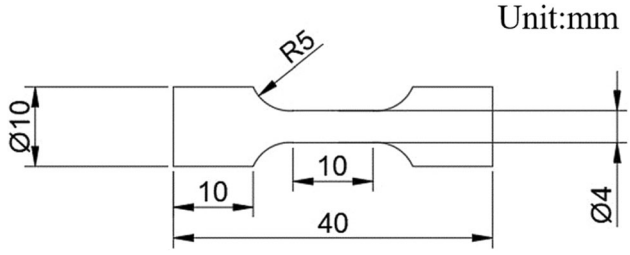

Fig. 1 Tensile specimen drawings

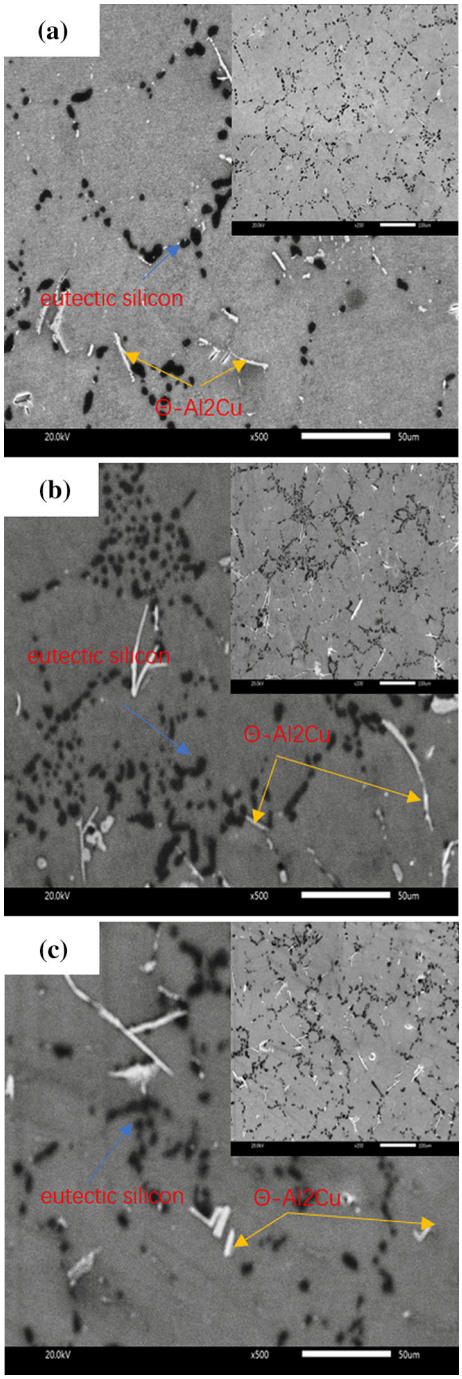

Fig. 2 SEM of Al-5Si-5.3Cu-0.3Sr-0.2Zr-0.2Y-0.06Ti-xMg alloy (a) #1; (b) #2; (c) #3

generate bulk Al_2Cu in the solid solution stage, which leads to a decrease in the solubility of Al_2Cu during the solid solution and increases the number of undissolved Al_2Cu after solution aging. According to Fig. 2(c) and 3, it can be seen that when 1% Mg is added, Cu is evenly distributed in the matrix and no large agglomeration is formed. Therefore, although the segregation of Cu is aggravated with the increase in the concentration of Mg, in the case of adding 0-1% Mg, the distribution of Cu in the matrix is still relatively uniform.

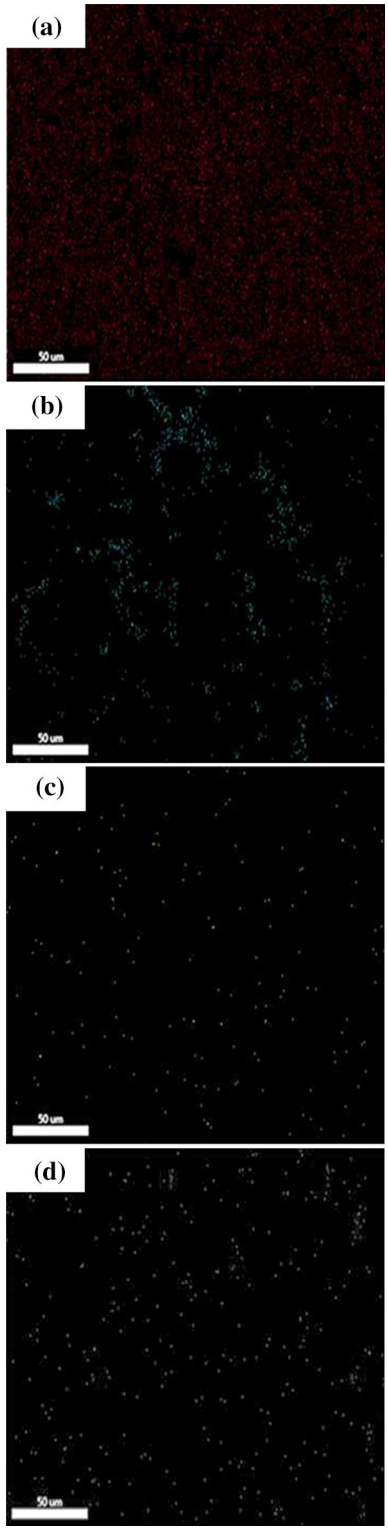

Fig. 3 EDS surface scan of Al-5Si-5.3Cu-0.3Sr-0.2Zr-0.2Y-0.06Ti-1 Mg alloy (a) Al; (b) Si; (c) Cu; (d) Mg

3.2 TEM Analysis

Figure 4 shows the TEM image for intragranular, θ' phase (FTT image) and Q′ phase (FTT image) of Al-5Si-5.3Cu-0.3Sr-0.2Zr-0.2Y-0.06Ti-*x*Mg ((a), (c), (e), the red circle is the θ'

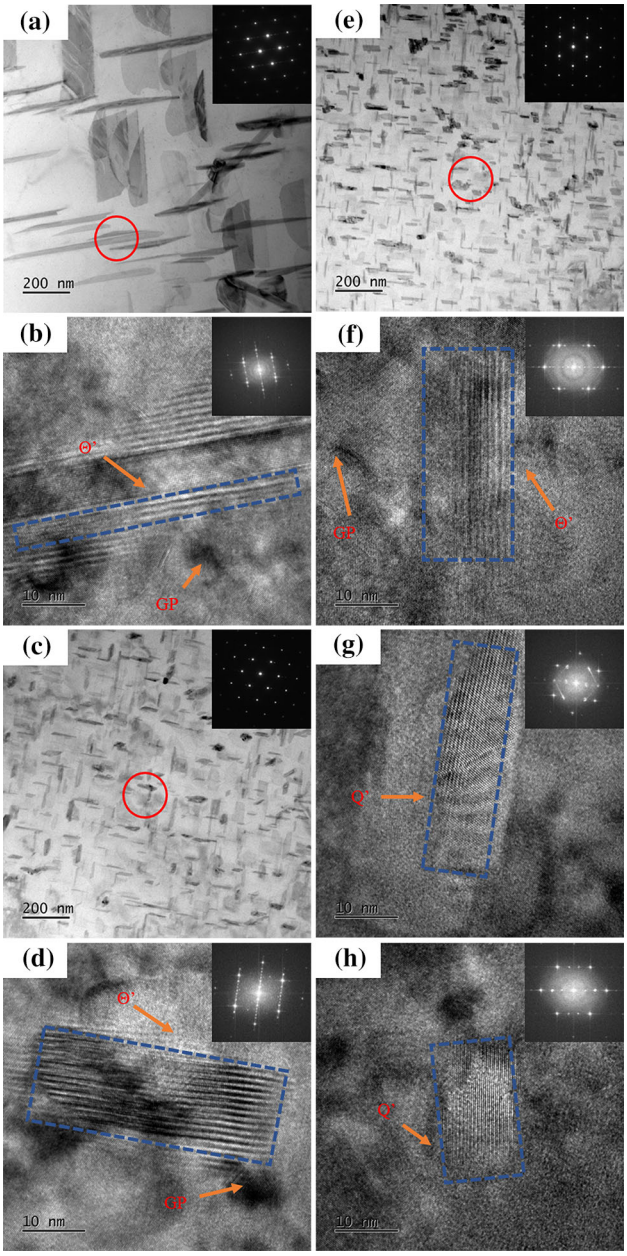

Fig. 4 TEM of Al-5Si-5.3Cu-0.3Sr-0.2Zr-0.2Y-0.06Ti-xMg alloy. (a) intragranular-TEM (SADP) of #1; (b) θ'-HRTEM(FFT) of #1; (c) intragranular-TEM (SADP) of #2; (d) θ'-HRTEM(FFT) of #2; (e) intragranular-TEM (SADP) of #3; (f) θ'-HRTEM(FFT) of #3; (g) Q′-HRTEM(FFT) of #2;(h) Q′-HRTEM(FFT) of #3

(Al_2Cu) precipitation). Table 2 presents the results of the average distance between adjacent θ' and θ' phase number density of Al-5Si-5.3Cu-0.3Sr-0.2Zr-0.2Y-0.06Ti-*x*Mg alloy as measured by ImageJ. Figure 4(a), (b), (c), (d), (e) and (f) shows that the precipitation in the alloy grains is mainly the θ' phase (Ref 17). As the magnesium addition increases, the size of the θ' phase reduces. In addition, the results of Fig. 4(a), (b), (c), (d), (e) and (f) and Table 2 show that the number density of the θ' phase in the alloy is found to increase as magnesium increases while the average distance of adjacent θ' phases is found to decrease as magnesium increases. It can be seen from Fig. 4(g) and (h) that the addition of magnesium also generates Q′ ($Al_5Cu_2Mg_8Si_6$) precipitate (Ref 11, 22-24), which is

Table 2 Average distance between adjacent θ' precipitates and θ' precipitates number density of Al-5Si-5.3Cu-0.3Sr-0.2Zr-0.2Y-0.06Ti-xMg alloy

Sample	Average distance between adjacent θ' precipitates, nm	θ' precipitates number density, μm^2
#1	128.6	21.7
#2	61.8	145.5
#3	46.7	230.3

rectangular in shape. And as the magnesium content increases, the size of the Q′ phase becomes smaller. Figure 5 shows the TEM images of PFZ and GBPs of Al-5Si-5.3Cu-0.3Sr-0.2Zr-0.2Y-0.06Ti-*x*Mg alloy (Ref 23, 25, 26). Figure 5 reveals that with the increase in magnesium content, the width of the PFZ is continuously narrowed, and the arrangement of GBPs along the PFZ is firstly discontinuously distributed, secondly continuously distributed, and finally discontinuously distributed (Ref 25).

The strengthening mechanism of θ' precipitate is consistent with the Orowan reinforcement model (Ref 27). Under this strengthening mechanism, the dislocation lines cannot directly cut through the θ' precipitate during plastic deformation. However, under the action of external force, the dislocation lines can bend around the θ' precipitate and finally leave a dislocation around the θ' precipitate loops, allowing dislocations to pass through. The bending of the dislocation line will increase the lattice distortion energy in the dislocation-affected zone, which increases the resistance to the movement of the dislocation line and increases the slip resistance (Ref 27, 28). As the resistance of dislocation movement increases, the obstacle to dislocation movement becomes larger, and the dislocation strengthening effect will be strengthened. The Orowan strengthening mechanism belongs to the second-phase strengthening mechanism in which the particles cannot be deformed. The reduction in the particle size of the second-phase precipitate, reduction in the distance between the second-phase precipitate, and the increase in the number density of the second-phase precipitate all increase the dislocation strengthening effect and the precipitation strengthening effect (Ref 12, 27, 29). According to the results of Fig. 4 and Table 2, the dislocation strengthening effect and the precipitation strengthening effect of the alloy increases with the increase in magnesium content. The Cu atoms will react with the Mg-Si atomic clusters first, so the Q′ phase will precipitate before the θ' phase, serving as a hindrance to dislocation movement (Ref 7), enhancing the dislocation strengthening effect. The small size of the generated Q′ precipitate is also beneficial to increasing the precipitation strengthening effect (Ref 12).

GBPs, PFZ, and adjacent matrix lead to the formation of micro-galvanic corrosion due to the potential differences, which results in the intergranular corrosion (Ref 23, 25, 26). When GBPs are continuously distributed, the formation of the continuous IGC path is easy, which increases IGC susceptibility (Ref 23, 25, 30). Therefore, changing the continuous distribution of GBPs helps to eliminate the IGC susceptibility and improve intergranular corrosion resistance. The more dispersed the distribution of GBPs is, the more difficult the forms of continuous corrosion channels is, and the stronger the intergranular corrosion resistance is Ref 25, 30, 31. In addition, the

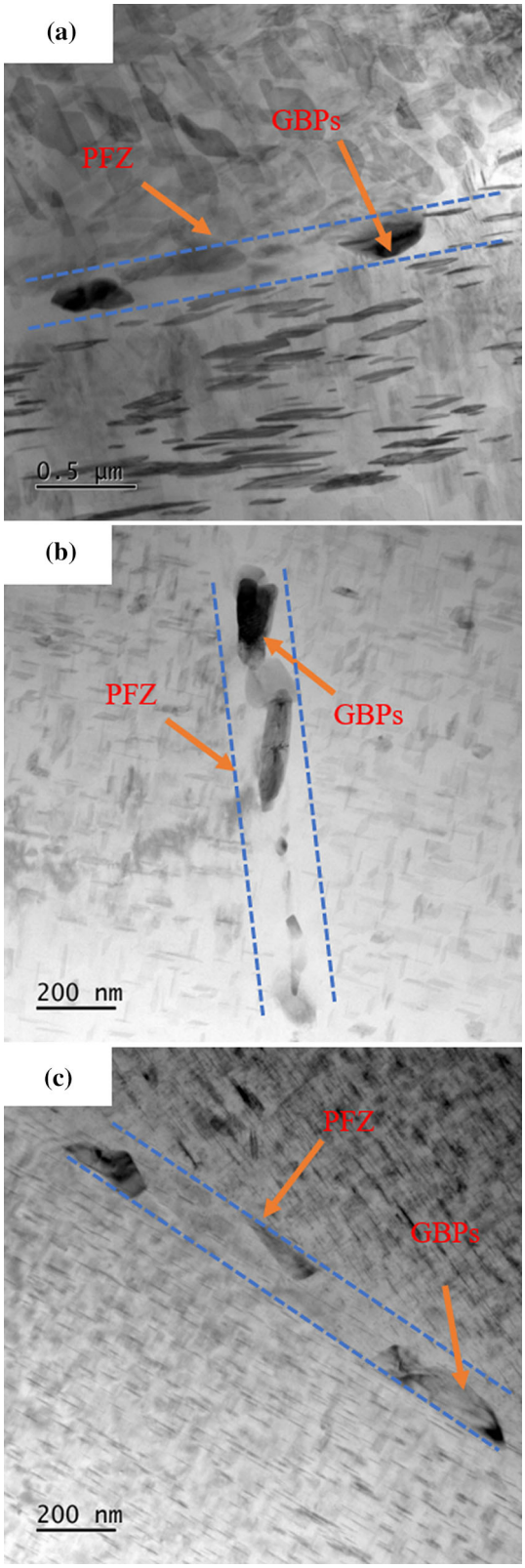

Fig. 5 TEM images of PFZ and GBPs of Al-5Si-5.3Cu-0.3Sr-0.2Zr-0.2Y-0.06Ti-xMg alloy (a) #1; (b) #2; (c) #3

smaller the width of PFZ is, the better the intergranular corrosion resistance of the alloy is Ref 25, 31.

Table 3 Tensile strength, hardness and elongation of Al-5Si-5.3Cu-0.3Sr-0.2Zr-0.2Y-0.06Ti-xMg alloy

Sample	Tensile strength, MPa	Elongation, %	Hardness, HV
#1	351.2	5.38	112.2
#2	291.1	4.92	122.5
#3	364.4	4.87	145.4

3.3 Performance Analysis

Table 3 shows the tensile strength, hardness, and elongation of Al-5Si-5.3Cu-0.3Sr-0.2Zr-0.2Y-0.06Ti-xMg alloy. With increased Mg content, the tensile strength of the alloy initially decreases and then increases, its hardness increases, and its elongation decreases.

The tensile strength of Al-Si-Cu alloys is affected by both undissolved particles and strengthened precipitates (Ref 12, 21, 27, 29). From the results in Fig. 2, it can be seen that #2 has more undissolved particles than #1. Therefore, #2 may have more macroscopic casting defects, which may result in premature fracture of the alloy during plastic deformation. Hence, Fig. 4 shows that the size of the θ' phase of the #2 after adding magnesium is smaller than #1 and its θ' number density is higher than that of #1, its dislocation strengthening and precipitation strengthening effects are better than those of #1, however, its tensile strength is far inferior to that of #1. Although the addition of 1% Mg increases the undissolved particles of #3, which may produce more casting defects than #1 and causes the alloy to fracture earlier in the plastic deformation stage. However, it further increases the number density of the θ' precipitation, reduces the distance between θ' particles, and reduces the size of the θ' precipitate. This further improves the precipitation strengthening effect of the alloy (Ref 27, 29). Moreover, adding magnesium generates the Q′ strengthening precipitation with a small size (Ref 7, 12), which improves the precipitation strengthening effect and dislocation strengthening of the alloy. Both of them improve the tensile strength of the alloy. At this time, the strengthening effect induced by precipitation strengthening and dislocation strengthening is the best, and #3 does not fracture early in the plastic deformation stage. Hence, the #3 has the highest tensile strength.

The plasticity of the alloy is mainly related to the brittle particle and the undissolved particle of the alloy (Ref 21, 32, 33). Combined with the results in Fig. 2, adding magnesium increases the number of undissolved particles in the alloy. The higher the number of undissolved particles, the worse the plasticity of the alloy. Since the addition of Mg causes the Cu phase to segregate (Ref 21), it increases the number of undissolved brittle θ precipitates (Ref 33, 34), which reduces the ductility of the alloy. Studies have shown that when magnesium is added to Al-Si-Cu alloy, the matrix transfers the high load on brittle phases already at small strains. It makes the brittle phases crack at low strains, which is also one of the reasons for the reduced elongation (Ref 32). Under the action of these two factors, the elongation of the alloy decreases continuously with the increase in Mg content, which is the same as the result of the previous study (Ref 6).

The increase in the hardness of the alloy is mainly related to the strengthening precipitation in the alloy (Ref 7, 15). The structure of the Q precipitate produces TM-Si bonds that lead to

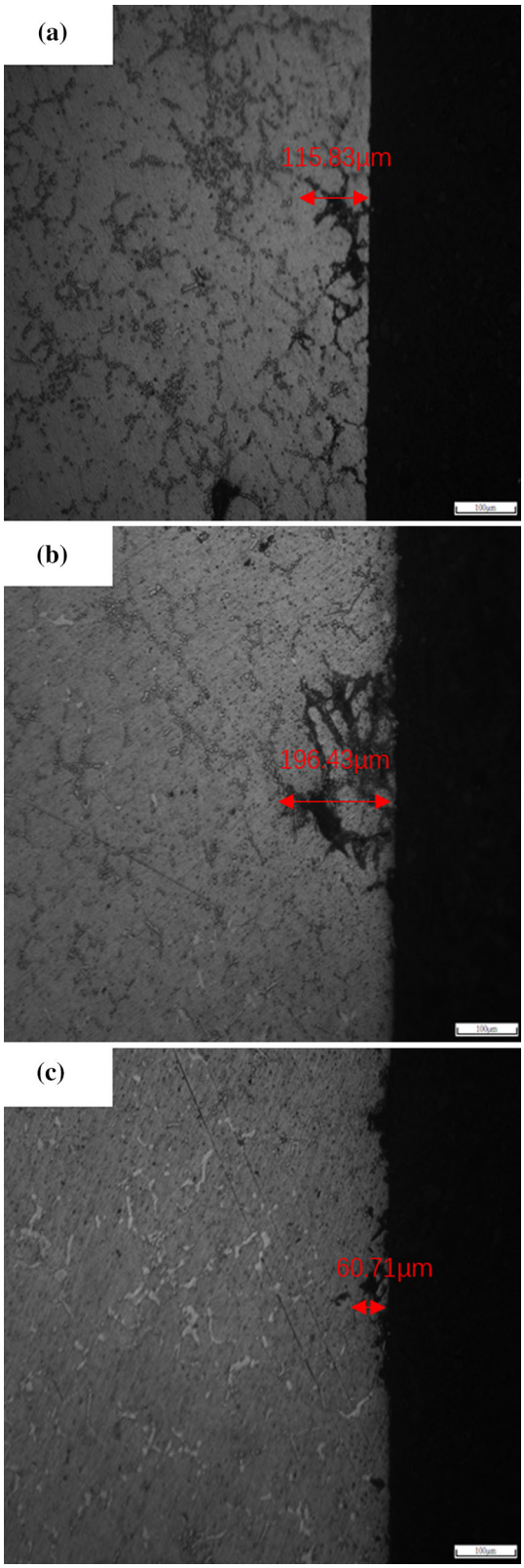

Fig. 6 OM diagram of intergranular corrosion of Al-5Si-5.3Cu-0.3Sr-0.2Zr-0.2Y-0.06Ti-xMg alloy (a) #1; (b) #2; (c) #3

an increase in hardness, and Q′, as a substance of the same chemical formula as the Q precipitation, may have similar properties (Ref 15). As the magnesium content increases, the size of Q′ precipitation becomes smaller, which improves the hardness of the alloy (Ref 7, 12). On the other hand, the addition of magnesium refines the size of θ' precipitate. The smaller the size of the θ' precipitate is Ref 12, the higher the hardness of the alloy is. Therefore, the hardness of the alloy increases as the magnesium content increases.

Table 4 Maximum intergranular corrosion depth and intergranular corrosion grades of Al-5Si-5.3Cu-0.3Sr-0.2Zr-0.2Y-0.06Ti-xMg alloy

Sample	Maximum intergranular corrosion depth, μm	Intergranular corrosion grade
#1	115.83	4
#2	196.43	4
#3	60.71	3

Figure 6 shows the OM images of Al-5Si-5.3Cu-0.3Sr-0.2Zr-0.2Y-0.06Ti-*x*Mg alloy after the IGC test. Table 4 shows the maximum IGC depth and IGC grade for Al-5Si-5.3Cu-0.3Sr-0.2Zr-0.2Y-0.06Ti-*x*Mg alloy. It can be seen from Fig. 6 and Table 4 that with the addition of magnesium, the intergranular corrosion depth of the alloy initially increases and then decreases. The intergranular corrosion resistance initially decreases and then increases with increased Mg content. This is consistent with the changes in PFZ and GBPs in the TEM of Fig. 5 (Ref 25, 30, 31). #2 has the worst resistance to intergranular corrosion. However, its width of PFZ becomes smaller after adding magnesium, which improves its resistance to intergranular corrosion. Notwithstanding, its GBPs are continuously distributed along PFZ, which easily forms corrosion channels and causes intergranular corrosion (Ref 30). Therefore, although the refinement of the width of PFZ improves its IGC resistance, its IGC resistance is the worst among the three samples due to the continuous distribution of its GBPs (Ref 25). And #3, with 1% Mg, the width of PFZ is further refined, and its GBPs distribution is dispersed, which reduces the probability of corrosion channel formation and improves the intergranular corrosion resistance, so its intergranular corrosion resistance is the best (Ref 25, 31).

4. Conclusions

(1) The high strength of the alloy is attributed to the precipitation strengthening phenomenon of the θ' and Q′ precipitates. The best precipitation strengthening effect of θ' and Q′ precipitates was attained at the addition of 1% Mg, with a tensile strength value of 364.4 MPa.
(2) The addition of magnesium changes the distribution of GBPs and the width of PFZ. The smallest width of PFZ was observed at the addition of 1% Mg, and the GBPs were discontinuously distributed at the same time. Therefore, the intergranular corrosion resistance reached its peak at this time, with the intergranular corrosion grade of 3.
(3) The enhanced hardness of the alloy is attributed to the refinement of θ' precipitate and the generation of Q′. The most significant hardness enhancement induced by

the θ' and Q′ precipitates was attained at the addition of 1% Mg, with a hardness value of 145.4 HV at this time.

Acknowledgments

The authors would like to acknowledge the financial support of Industrial Science and technology support program of Jiangsu province (Grant No. BE2008118), and the Key Projects of the 13th Five-Year Plan Equipment Pre-research Foundation of the Ministry of Equipment Development of the Central Military Commission of China (No. 6140922010201).

References

1. S. Mondol, U. Bansal, M.P. Singh, S. Dixit, A. Mandal, A. Paul, and K. Chattopadhyay, Microstructure-Strength Correlations in Al-Si-Cu Alloys Micro-Alloyed with Zr, *Materialia*, 2022, **23**, 101449.
2. M.H. Abdelaziz, A.M. Samuel, H.W. Doty, V. Songmene, and F.H. Samuel, Mechanical Performance and Precipitation Behavior in Al-Si-Cu-Mg Cast Alloys: Effect of Prolonged Thermal Exposure, *Materials*, 2022, **15**(8), p 2830.
3. D. Bolibruchová, L. Širanec, and M. Matejka, Selected Properties of a Zr-Containing AlSi5Cu2Mg Alloy Intended for Cylinder Head Castings, *Materials*, 2022, **15**(14), p 4798.
4. Z.P. Shi, R.H. He, Y. Chen, H. Yan, H.G. Song, C. Luo, Q. Nie, and Z. Hu, Microstructural Evolution and Strengthening Mechanisms of a Novel Al-11Si-3Cu Alloy microalloyed with Minor Contents of Sr and Sc, *Mater. Sci. Eng. A*, 2022, **853**, 143738.
5. A. Lombardi, F. D'Elia, C. Ravindran, and R. Mackay, Replication of Engine Block Cylinder Bridge Microstructure and Mechanical Properties with Lab Scale 319 Al Alloy Billet Castings, *Mater. Charact.*, 2014, **87**, p 125–137.
6. A.R. Farkoosh, and M. Pekguleryuz, Enhanced Mechanical Properties of an Al-Si-Cu-Mg Alloy at 300 °C: Effects of Mg and the Q-Precipitate Phase, *Mater. Sci. Eng. A*, 2015, **621**, p 277–286.
7. N. Fang, C.M. Zou, Z.J. Wei, H.W. Wang, X.J. Zhang, and T. Chang, Effect of Ge and Mg Additions on the Aging Response Behavior and Mechanical Properties of Al-Si-Cu Alloy, *Mater. Sci. Eng. A*, 2021, **811**, 141024.
8. M.S. Salleh, M.Z. Omar, and J. Syarif, The Effects of Mg Addition on the Microstructure and Mechanical Properties of Thixoformed Al–5%Si–Cu Alloys, *J. Alloy. Compd.*, 2015, **621**, p 121–130.
9. X.Z. Zhu, X.X. Dong, P. Blake, and S.X. Ji, Improvement in As-Cast Strength of High Pressure Die-Cast Al–Si–Cu–Mg Alloys by Synergistic Effect of Q-$Al_5Cu_2Mg_8Si_6$ and θ-Al_2Cu Phases, *Mater. Sci. Eng. A*, 2021, **802**, 140612.
10. D.J. Chakrabarti, and D.E. Laughlin, Phase Relations and Precipitation in Al-Mg-Si Alloys with Cu Additions, *Prog. Mater Sci.*, 2004, **49**(3–4), p 389–410.
11. Y. Zheng, W.L. Xiao, S.J. Ge, W.T. Zhao, S.J. Hanada, and C.L. Ma, Effects of Cu Content and Cu/Mg Ratio on the Microstructure and Mechanical Properties of Al–Si–Cu–Mg Alloys, *J. Alloy. Compd.*, 2015, **649**, p 291–296.
12. J.F. Hao, B.Y. Yu, J.C. Bian, L. Zheng, S.N. Nie, and R.X. Li, Comparison of the Semisolid Squeeze Casting and Gravity Casting Process on the Precipitation Behavior and Mechanical Properties of the Al-Si-Cu-Mg Alloy, *Mater. Charact.*, 2021, **180**, 111404.
13. Y. Zou, Q. Liu, Z.H. Jia, Y. Xing, L.P. Ding, and X.L. Wang, The Intergranular Corrosion Behavior of 6000-Series Alloys with Different Mg/Si and Cu Content, *Appl. Surf. Sci.*, 2017, **405**, p 489–496.
14. Q. Xiao, H.Q. Liu, D.Q. Yi, D.Y. Yin, Y.Q. Chen, Y. Zhang, and B. Wang, Effect of Cu Content on Precipitation and Age-Hardening Behavior in Al-Mg-Si-xCu Alloys, *J. Alloy. Compd.*, 2017, **695**, p 1005–1013.
15. Y.F. Ouyang, F.L. Liu, T. Lu, X.M. Tao, Y. Du, and Y.H. He, First Principles investigation of the Mechanical, Electronic and Thermophysical Properties of Q-Phase in Al–Mg–Si–Cu Alloys, *Comput. Mater. Sci.*, 2013, **67**, p 334–340.
16. Z.J. Wang, M. Zhang, Q.Y. Zhang, and J.Q. Lv, Strengthening Mechanism of Compositely Refined and Modified Multi-component Aluminum-Silicon Alloy, *Rare Metal Mater. Eng.*, 2020, **49**(10), p 3402–3411.
17. T.K. Akopyan, N.A. Belov, N.V. Letyagin, F.O. Milovich, A.A. Lukyanchuk, and A.S. Fortuna, Influence of Indium Trace Addition on the Microstructure and Precipitation Hardening Response in Al–Si–Cu Casting Aluminum alloy, *Mater. Sci. Eng. A*, 2022, **831**, 142329.
18. S. Bahl, J.U. Rakhmonov, C. Kenel, D.C. Dunand, and A. Shyam, Effect of Grain-Boundary θ-Al_2Cu Precipitates on Tensile and Compressive Creep Properties of Cast Al–Cu–Mn–Zr Alloys, *Mater. Sci. Eng. A*, 2022, **840**, 142946.
19. A.R. Farkoosh, M. Javidani, M. Hoseini, D. Larouche, and M. Pekguleryuz, Phase Formation in as-Solidified and Heat-Treated Al-Si-Cu-Mg-Ni Alloys: Thermodynamic Assessment and Experimental Investigation for Alloy Design, *J. Alloy. Compd.*, 2013, **551**, p 596–606.
20. G.L. Mao, C.C. Zhu, S. Wang, H. Yan, and W.L. Gao, The Role of Yttrium Modifying A357 Alloy with Sand Casting, *Mater. Sci. Technol.*, 2019, **35**(15), p 1815–1821.
21. A.M.A. Mohamed, M.F. Ibrahim, E. Samuel, A.M. Samuel, F.H. Samuel, H.W. Doty, Assessment of the Effect of Mg Addition on the Solidification behavior, Tensile and Impact Properties of Al–Si–Cu Cast Alloys. Int. J. Metalcast., pp. 1–27 (2022)
22. W.C. Yang, S.X. Ji, Z. Li, and M.P. Wang, Grain Boundary Precipitation Induced by Grain Crystallographic Misorientations in an Extruded Al–Mg–Si–Cu Alloy, *J. Alloy. Compd.*, 2015, **624**, p 27–30.
23. Z.X. Wang, F. Zhu, K. Zheng, J. Jia, Y.L. Wei, H. Li, L.P. Huang, and Z.Q. Zheng, Effect of the Thickness Reduction on intergranular Corrosion in an Under-Aged Al-Mg-Si-Cu Alloy During cold-Rolling, *Corros. Sci.*, 2018, **142**, p 201–212.
24. W.C. Yang, L.P. Huang, R.R. Zhang, M.P. Wang, Z. Li, Y.L. Jia, R.S. Lei, and X.F. Sheng, Electron Microscopy Studies of the Age-Hardening Behaviors in 6005A Alloy and Microstructural Characterizations of Precipitates, *J. Alloy. Compd.*, 2012, **514**, p 220–233.
25. X. Zhan, J.G. Tang, H.Z. Li, X.P. Liang, Y.F. Lu, Y.X. Che, W.B. Tu, and Y.D. Zhang, Effects of Non-isothermal Aging on Mechanical Properties, Corrosion Behavior and Microstructures of Al-Cu-Mg-Si Alloy, *J. Alloys Compd*, 2020, **819**, p 152960.
26. C. Schnatterer, C. Altenbach, and D. Zander, The Effect of Simulated In-Service Heat Impact on the Microstructure and Corrosion Properties of a High Cu Containing Al-Mg-Si Alloy, *Mater. Corros.*, 2019, **70**(7), p 1205–1213.
27. J.F. Nie, and B.C. Muddle, Strengthening of an Al-Cu-Sn Alloy by Deformation-Resistant Precipitate Plates, *Acta Mater.*, 2008, **56**(14), p 3490–3501.
28. Y. Hu, and W.A. Curtin, Modeling of Precipitate Strengthening with Near-Chemical Accuracy: Case Study of Al-6xxx Alloys, *Acta Mater.*, 2022, **237**, 118144.
29. H.X. Cao, Q.C. Sun, Q.Q. Pu, L.H. Wang, M.T. Huang, Z.W. Luo, and J.Q. Che, Effect of Vacuum Degree and T6 Treatment on the Microstructure and Mechanical Properties of Al–Si–Cu Alloy Die Castings, *Vacuum*, 2020, **172**, 109063.
30. X.M. Zhang, L. Liu, L.Y. Ye, J. Liu, Z. Lei, and J.C. Song, Effect of Pre-deformation of Rolling Combined with Stretching on Stress Corrosion of Aluminum Alloy 2519A Plate, *Trans. Nonferrous Met. Soc. China*, 2012, **22**(1), p 8–15.
31. X.Y. Peng, Q. Guo, X.P. Liang, Y. Deng, Y. Gu, G.F. Xu, and Z.M. Yin, Mechanical Properties, Corrosion Behavior and Microstructures of a Non-isothermal Ageing treated Al-Zn-Mg-Cu Alloy, *Mater. Sci. Eng. A*, 2017, **688**, p 146–154.
32. C.H. Caceres, I.L. Svensson, and J.A. Taylor, Strength-Ductility Behaviour of AI-Si-Cu-Mg Casting Alloys in T6 Temper, *Int. J. Cast Met. Res.*, 2003, **15**(5), p 531–543.
33. M. Zeren, E. Karakulak, and S. Gümüş, Influence of Cu Addition on Microstructure and Hardness of Near-Eutectic Al-Si-xCu-Alloys, *Trans. Nonferrous Met. Soc. China*, 2011, **21**(8), p 1698–1702.
34. M.S. Zhang, K.L. Liu, J.Q. Han, F. Qian, J.S. Wang, and S.K. Guan, Investigating the Role of Cu, Zr and V on the Evolution of Microstructure and Properties of Al-Si-Mg Cast Alloys, *Mater. Today Commun.*, 2021, **26**, 102055.

Publisher's Note Springer Nature remains neutral with regard to jurisdictional claims in published maps and institutional affiliations.